Registration of Remote Sensing Image Data Based on Wavelet Transform

Mitsuyoshi Tomiya   and   Akihiro Ageishi

Department of Applied Physics, Seikei University, Kichijoji-Kitamachi 3-3-1, Musasino-shi, Tokyo, 180-8633, Japan - tomiya@apm.seikei.ac.jp

Abstract:

A registration method of remotely sensed image data which is base on the wavelet transform is proposed.   The shape information of the regions in the images is analyzed by the Haar and Daubechies' wavelets.   Comparing the coefficients of the wavelets and minimizing the mean square error (MSE) which is defined by the coefficients, the regions are matched and the images are registered. Affine transformation is applied for the registration and its parameters are also determined by the minimum of the MSE.   Our result shows that the wavelet method is remarkably stable, irrespective of various shapes of the regions.

WG II/IV, III/4, III/5, III/6

Keywords: Registration, Haar wavelet transform, Daubechies' wavelet transform, Affine transform, Fourier descriptor

1．Introduction

Registration technique is necessary for geometrical matching of the remote sensing images. It makes possible to monitor natural and artificial changes in land cover precisely.   We have studied the Fourier descriptor method that is applied to the feature of the regions on the data (Anzai and Tomiya, 2001).   The Fourier descriptors represent the shapes of the boundaries and are compared to be matched and then registered.   However this method is very applicable only for round shaped regions.   Here we propose an alternative method which is based on the wavelet transform, which has also been adopted for remote sensing data last decade(e.g. (Simhadri, 1998)).

For the image registration, it is necessary to extract and compare the image features.   There are various kinds of image features: shapes, distributions (of brightness, colors,…), textures, etc. Among them the shape information must be the most robust and the most effective for the remote sensing data under various conditions.   Generally the edge detection is applied to get the pixels of the boundaries that from the shape features.   In this work, it is very important that the extracted boundaries are surely connected.   Therefore the region growing is applied to the characteristic regions of the images after the segmentation. Then the edge detection is adopted to extract the boundaries of the regions as the shape information of the images.

2.　Fourier descriptor and affine transform

2-1 Fourier descriptor

After the edge extraction, the image feature is represented as a one-dimensional close curve in two dimensional image.   Setting a start point, a distance t is introduced along the curve.

Normalizing the distance of the perimeter 2π, the coordinates (x, y) of the points on the curve can be considered as the periodic functions

$$x(t + 2\pi) = x(t) , \quad y(t + 2\pi) = y(t) \quad (0 \le t < 2\pi) . \quad (1)$$

We present $x(t)$ and $y(t)$ of the closed curve in the x-y plane (image) as the function of t ($0 \le t \le 2\pi$).   The Fourier transforms of the coordinates (x, y) are

$$\begin{pmatrix} x(t) \\ y(t) \end{pmatrix} = \begin{pmatrix} a_0 \\ c_0 \end{pmatrix} + \sum_{k=1}^{\infty} \begin{pmatrix} a_k & b_k \\ c_k & d_k \end{pmatrix} \cdot \begin{pmatrix} \cos kt \\ \sin kt \end{pmatrix} , \quad (2)$$

$$a_0 = \frac{1}{2\pi} \int_0^{2\pi} x(t)\,dt, \quad c_0 = \frac{1}{2\pi} \int_0^{2\pi} y(t)\,dt,$$

$$a_k = \frac{1}{\pi} \int_0^{2\pi} x(t)\cos kt\,dt, \quad b_k = \frac{1}{\pi} \int_0^{2\pi} x(t)\sin kt\,dt,$$

$$c_k = \frac{1}{\pi} \int_0^{2\pi} y(t)\cos kt\,dt, \quad d_k = \frac{1}{\pi} \int_0^{2\pi} y(t)\sin kt\,dt,$$

where a_k, b_k, c_k, d_k are the coefficients of the k-th Fourier series or called the k-th Fourier descriptors (Granlund, 1972, Zahn and Roskies, 1972), especially a_0, c_0 are the center of gravity.

2-2 Affine transform and mean square error

To register the images, the geometrical distortion which is mainly due to the satellite attitude and altitude, etc. have to be detected and adjusted.   In general it may cause parallel transform, rotation, expansion-reduction and also skew transform etc. of the image.   Here we choose the affine transform to adjust the images.   Appling the affine transform to the image A with the coordinates (x, y) to be matched to the image A$'$ with (x', y'),

we have

$$\begin{pmatrix} x' \\ y' \end{pmatrix} = \begin{pmatrix} \alpha & \beta \\ \gamma & \delta \end{pmatrix} \cdot \begin{pmatrix} x \\ y \end{pmatrix} + \begin{pmatrix} \Delta x \\ \Delta y \end{pmatrix} \quad , \quad (\alpha\delta - \beta\gamma \neq 0) \tag{4}$$

where $\alpha, \beta, \gamma, \delta, \Delta x, \Delta y$ are the constants. The coefficients $\alpha, \beta, \gamma, \delta$ form the affine transform and include rotation, expansion-reduction, skew transform and $\Delta x, \Delta y$ are the displacement to be parallel transformed.

Applying the Fourier transform (2) to Eq.(4), the transform rules of the Fourier descriptors for (x,y) to the descriptor a'_k, b'_k, c'_k, d'_k for (x',y') are derived as

$$\begin{pmatrix} a'_k & b'_k \\ c'_k & d'_k \end{pmatrix} = \begin{pmatrix} \alpha & \beta \\ \gamma & \delta \end{pmatrix} \cdot \begin{pmatrix} a_k & b_k \\ c_k & d_k \end{pmatrix}, \tag{5}$$

$$\begin{pmatrix} a'_0 \\ c'_0 \end{pmatrix} = \begin{pmatrix} \alpha & \beta \\ \gamma & \delta \end{pmatrix} \cdot \begin{pmatrix} a_0 \\ c_0 \end{pmatrix} + \begin{pmatrix} \Delta x \\ \Delta y \end{pmatrix}. \tag{6}$$

Actually the coarse feature of the shape which belongs to the coefficients $k \leq 2$ is sufficient for the matching (Tseng et.al., 1997; Anzai and Tomiya, 2001). For realistic digital image, Eq.(5) cannot be exactly satisfied. There are always errors in the calculated coefficients. The mean square error (MSE) for the affine coefficients is defined as

$$MSE_F = \frac{1}{n} \sum_{k=1}^{n} \left(\varepsilon_{a,k}{}^2 + \varepsilon_{b,k}{}^2 + \varepsilon_{c,k}{}^2 + \varepsilon_{d,k}{}^2 \right), \tag{7}$$

where the errors for the coefficients are

$$\begin{pmatrix} \varepsilon_{a,k} & \varepsilon_{b,k} \\ \varepsilon_{c,k} & \varepsilon_{d,k} \end{pmatrix} = \begin{pmatrix} a'_k & b'_k \\ c'_k & d'_k \end{pmatrix} - \begin{pmatrix} \alpha & \beta \\ \gamma & \delta \end{pmatrix} \cdot \begin{pmatrix} a_k & b_k \\ c_k & d_k \end{pmatrix}. \tag{8}$$

Varying the affine parameters, the minimum of the MSE_F for the fixed Fourier descriptors determines the matching transform.

3. Wavelet transformation

3-1 Wavelet

The wavelet is defined as the superposition of the wave which has local support (Stollnitz et.al., 1996). Its fundamental waves are the mother wavelet $\Psi(t)$ and the scaling function (or the father wavelet) $\phi(t)$. The wavelet transform is to expand the original wave into these two kinds of waves. The mother wavelet and the scaling function obey three following rules.

1) Two-scale relation

The mother wavelet and the scaling function are defined by the reconstruction sequences $\{p_k\}$ and $\{q_k\}$,

$$\Psi(t) = \sum_k q_k \phi(2t - k),$$

$$\phi(t) = \sum_k p_k \phi(2t - k) \quad (k: \text{integer}). \tag{9}$$

2) Admissibility condition

Integration of the mother wavelet in the range that includes its whole support must vanish

$$\int_{-\infty}^{\infty} \Psi(t)\, dt = 0. \tag{10}$$

It is the fundamental condition for the wavelet and also called the wavelet condition.

3) Orthogonal condition

The mother wavelet and the scaling function own the orthogonal relation,

$$\langle \phi(t-m), \phi(t-n) \rangle = c\delta_{m,n} \quad (m,n: \text{integer})$$
$$\langle \Psi(t-m), \Psi(t-n) \rangle = c\delta_{m,n}$$
$$\langle \Psi(t-m), \phi(t-n) \rangle = 0 \quad , \tag{11}$$

where $\langle \cdots, \cdots \rangle$ denotes the inner product of the wavelet function space

$$\langle \alpha(t), \beta(t) \rangle = \int_{-\infty}^{\infty} \alpha^*(t)\beta(t)dt. \tag{12}$$

In Eq.(11), m and n represent the displacement in t. The scaling functions with the different displacements are orthogonal. The mother wavelets with the different displacements are also orthogonal. The mother wavelet and the scaling function are always orthogonal. It leads us to the relation for the sequences $\{p_k\}$ and $\{q_k\}$

$$q_k = (-1)^k p_{1-k}. \tag{13}$$

Setting $c=1$, the mother wavelet and the scaling function form the orthonormal system. Then the system of Eq.(11) is called the orthonormal wavelet.

3-2 Haar wavelet

The wavelet made of the Haar function is the simplest one. The mother wavelet and the scaling function (Fig.1) are defined as

$$\Psi(t) = \begin{cases} 1 & (0 \leq t \leq 1/2) \\ -1 & (1/2 \leq t \leq 1) \\ 0 & (otherwise) \end{cases}, \tag{14}$$

$$\phi(t) = \begin{cases} 1 & (0 \leq t \leq 1) \\ 0 & (otherwise) \end{cases}, \tag{15}$$

The system obeys the three conditions (9), (10), (11) and $c=1$.

The decomposition algorithm of the Haar wavelet is

$$c_k^{(j+1)} = \frac{1}{2}(c_{2k}^{(j)} + c_{2k+1}^{(j)}),$$

$$d_k^{(j+1)} = \frac{1}{2}(c_{2k}^{(j)} - c_{2k+1}^{(j)}), \tag{16}$$

where $j \geq 0$. At first $\left\{c_k^{(0)}\right\}$ is set the consecutive coodinate values on the boundary. The wavelet coefficient $c_k^{(j+1)}$ after the decomposition becomes the average value of its neighboring wavelet coefficients $c_{2k}^{(j)}$ and $c_{2k+1}^{(j)}$, and $d_k^{(j+1)}$ is the difference of them. To reconstruct the original data, we can use the reconstruction algorithm

$$c_{2k}^{(j)} = c_k^{(j+1)} + d_k^{(j+1)},$$

$$c_{2k+1}^{(j)} = c_k^{(j+1)} - d_k^{(j+1)}. \tag{17}$$
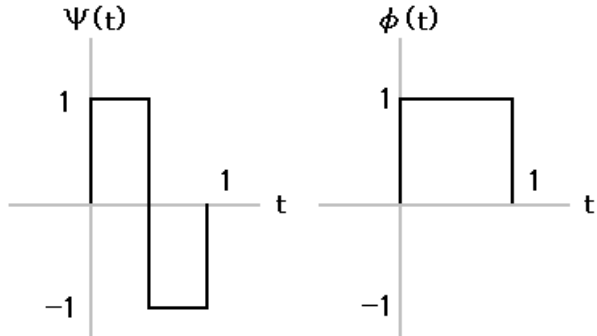
Fig.1 The mother wavelet $\Psi(t)$ and the scaling function $\phi(t)$ form the Haar wavelet.

3-3 Daubechies' wavelet

I. Daubechies found the system of the wavelet functions with $2N$ coefficients (Daubechies, 1998, 1992). Haar wavelet functions themselves are defined not to overlap each other. On the other hand, Daubechies' wavelet functions overlap each other to some degree and interpolate together. Still they are orthogonal.

Daubechies' wavelet is defined by the conditions of the two-scale sequence $\{ p_k \}$ which plays the key role in the two-scale relation of the scaling function:

$$\left\{ \begin{array}{l} \displaystyle\sum_{k=0}^{2N-1} p_k = \sqrt{2} \\ \displaystyle\sum_{k=0}^{2N-1} p_k^2 = 1 \\ \displaystyle\sum_{k=0}^{2N-1} p_k p_{k+2n} = 0 \quad (n \neq 0) \end{array} \right. \tag{18}$$

Here N is called the Daubechies' parameter and only $2N$ ones are non-zero (Daubechies, 1998, 1992). When $N=1$, it is the same as the Haar wavelet. The larger N becomes, the stronger the interpolation operates. The resolution of the image also improves, though; inevitably the computational complexity grows rapidly.

The mother wavelet and the scaling function for the Daubechies 2 (Fig. 2) have the overlaps in more complicated way than the Haar wavelet and they interpolate each other. In this work, we choose Daubechies 2 wavelet whose decomposition algorithm is

$$c_k^{(j+1)} = \frac{1}{8}\left\{(1+\sqrt{3})c_{2k}^{(j)} + (3+\sqrt{3})c_{2k+1}^{(j)} + (3-\sqrt{3})c_{2k+2}^{(j)} + (1-\sqrt{3})c_{2k+3}^{(j)}\right\}, \tag{19}$$

$$d_k^{(j+1)} = \frac{1}{8}\left\{(1-\sqrt{3})c_{2k}^{(j)} - (3-\sqrt{3})c_{2k+1}^{(j)} + (3+\sqrt{3})c_{2k+2}^{(j)} - (1+\sqrt{3})c_{2k+3}^{(j)}\right\}.$$
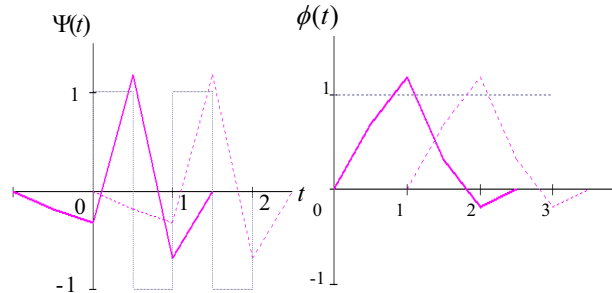
Fig.2 The mother wavelet and the scaling function for the Daubechies 2.

3-4 Mean square error

We adopt the coordinates (x, y) of the boundary in the image A as the level-0 wavelet coefficients $\left(c_{x,k}^{(0)}, c_{y,k}^{(0)}\right)$, where k denotes the number of pixels from the starting point of the boundary. The wavelet transform (Eq.(16) or Eq.(19)) is applied and get higher level coefficients $\left(c_{x,k}^{(j)}, c_{y,k}^{(j)}\right)$ and $\left(d_{x,k}^{(j)}, d_{y,k}^{(j)}\right)$. As in section 2 we also compare the lower frequency components of image A and images A′. The term $d_{x(y),k}^{(j)}$ also has the information of the feature, however, it usually has only fine variation of the feature. Thus we choose the term $c_{x(y),k}^{(j)}$ for the matching. We can also define the MSE, which is to be minimized for the matching process. Because the coefficients are just the "averaged" coordinate value of region boundaries, there is similar relation between $c_{x(y),k}^{(j)}$ of image A and $c_{x(y),k}'^{(j)}$ of image A′ by the affine transform and the errors for the coefficients are defined as

$$\begin{pmatrix} \varepsilon_{x,k}^{(j)} \\ \varepsilon_{y,k}^{(j)} \end{pmatrix} = \begin{pmatrix} c_{x,k}'^{(j)} \\ c_{y,k}'^{(j)} \end{pmatrix} - \left[\begin{pmatrix} \alpha & \beta \\ \gamma & \delta \end{pmatrix} \cdot \begin{pmatrix} c_{x,k}^{(j)} \\ c_{y,k}^{(j)} \end{pmatrix} + \begin{pmatrix} \Delta x \\ \Delta y \end{pmatrix} \right], \tag{20}$$

and the MSE for the wavelet transform is

$$MSE_W^{(j)} = \frac{1}{2n} \sum_{k=0}^{n} \left\{ (\varepsilon_{x,k}^{(j)})^2 + (\varepsilon_{y,k}^{(j)})^2 \right\}. \tag{21}$$

In the same manner as the Fourier descriptor, the parameters α, $\beta, \gamma, \delta, \Delta x, \Delta y$ that minimize $MSE_W^{(j)}$ determine the affine transform for the matching. Actually for the remote sensing image data, it is found that it works efficiently only at about $j \leq 3$, higher level does not improve the result very much.

4. Result and discussions

Our method of the registration is tested by the data of Hachirogata lake, Akita prefecture, Japan (Fig.3) which was taken by Landsat 5 and the data of Sapporo city, Hokkaido prefecture(Fig.5) by Ikonos. The spatial resolution of the thematic mapper on Landsat 5 is 30 meter and the resolution of the multi-spectral sensor on Ikonos is 4 meter. We prepare the original images and its rotated ones as the test images to be registered. At first we assign the regions in the test image which are assumed to be the same regions in the original image. Then the reliability of the registration is evaluated by the MSE. The image of Hachirogata lake has large portion of water body. The separation of water body and land is relatively straightforward to introduce the infrared band (TM4). On the other hand the image of Sapporo city has little water body and we choose artificially shaped buildings to be the feature regions.

The evaluation of the matching by the wavelet is owing to $MSE_W^{(3)}$ which is made of the level-3 wavelet coefficients $c_k^{(3)}$. As in the section 3, smaller MSE means more probable matching pair of regions. The most of pairs of the same regions have less than 1 (Table 1, 2). It implies that the accuracy of registration is less than one pixel. The affine transform is just a combination of linear transforms, however, the accuracy is good enough to register the remote sensing data. The most of pairs of the different regions are larger than 10(Table 3). Thus the threshold value can be set in between these values, such as 4.

Generally the mean square error of the Haar wavelet is smaller than the mean square error of the Daubechies' wavelet. Exceptionally, $MSE_W^{(3)}$ of several pairs of the same regions are preferably larger value. Especially the pair [7-g] in Hachirougata lake (Table 1) and the pair [4-d] in Sapporo city (Table 2) have larger value than expected. In the case of Hachirogata lake, the region [5] in the original image and the region [e] in the test image are apparently belong to the same region, unfortunately their extracted shapes are considerably different. However, the *MSE*s are just in the middle of matched pairs and non-matched pairs. In spite of the large difference between the MSEs of the pair [7-g] of Hachirogata lake, their extracted shapes have no clear difference. It would be due to their small sizes. The larger MSE of the pair [1-a] of Hachirogata lake must be due to their complicated shapes.

In table 2 of Sapporo city, the pair [1-a] is not likely to have the large MSE, because their shape is not very complicated and can be easily distinguished manually. Our method has also the effect of the low-pass filter that would reduce the noise on the

shape information. This region is actually the largest object in our image. The shape is larger, the registration seems more free from noise. The number of pixels of [1] is 366, on the other hand, the region [a] has 418 pixels on its longer perimeter. We enlarge the number of pixels on shorter perimeter region by simple interpolation. Their difference is about 15% and would be large enough to generate the noise and to affect the result.

Fig.3 Landsat true-color image of Hachirogata lake, Japan at 28 Apr. 1988: Spring data. (left：the original image, right：the test image).
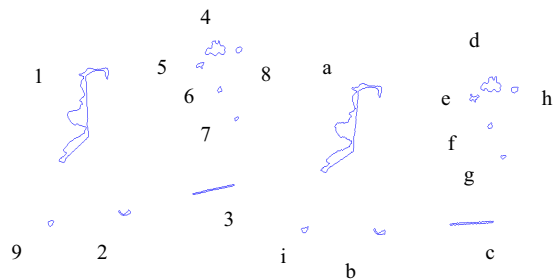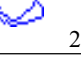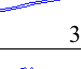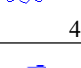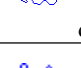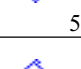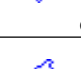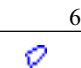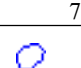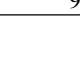
Fig.4 Feature regions in Fig.3.

Table.1 MSE_W of the feature regions of Fig.4 (1.2,.. means the region in the original image and alphabet is in the test image).

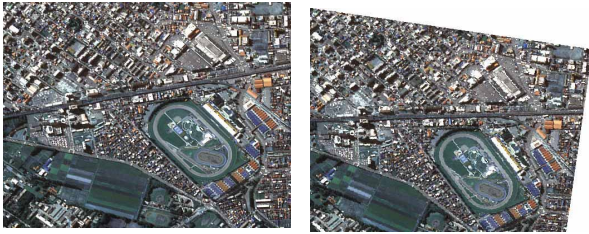| Original image	Test image	*MSE*(Haar)	*MSE*(Daubechies2)
1	a	1.268	1.284
2	b	0.462	0.517
3	c	0.480	0.488
4	d	0.799	0.836
5	e	1.558	1.584
6	f	0.571	0.606
7	g	1.715	3.068
8	h	0.840	0.778
9	i	0.578	0.602

Fig.5   Ikonos true-color image of Sapporo city, Japan at 8 May 2000.
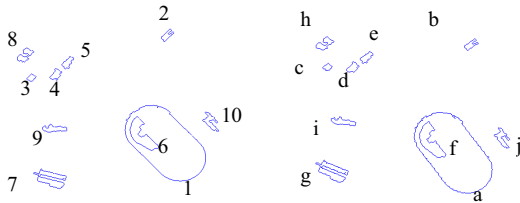（left：the original image, right：the test image）
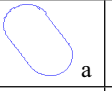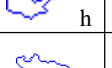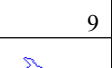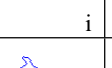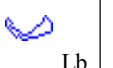
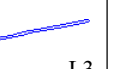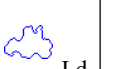Fig.6   Feature regions in Fig.5.

Table.2 MSE_W of the feature regions of Fig.6 (1,2,.. means the region in the original image and alphabet is in the test image).

Original	Test	MSE_W(Haar)	MSE_W(Daubechies2)
1	a	2.654	2.657
2	b	0.603	0.617
3	c	0.814	0.901
4	d	1.179	1.233
5	e	0.684	0.990
6	f	0.854	0.961
7	g	0.570	0.567
8	h	0.672	0.564
9	i	0.587	0.598
10	j	0.861	0.865

For the pair [7-g] of Hachirogata lake, the Daubechies MSE is much larger than the Haar MSE. The pair is the smallest one in our images. Theoretical inspection may predict that the Daubechies' wavelet is more sophisticated and more effective, because the effect of the interpolation is stronger. The Daubechies' wavelet require 4 consecutive pixels to decompose, while the Haar wavelet needs 2 neighboring pixels. The interpolation would cause reverse effect for smaller region, which

Table.3 MSE_W of the pairs of apparently non matched regions. Labels of the regions that start with 'L' are the regions in the Landsat data (Hachirogata lake): Fig.4 and start with I are in the Ikonos data (Sapporo city): Fig.6. (For example L5= Region [5] in Fig.4).

Original	Test	MSE_W(Haar)	MSE_W(Daubechies2)
L5	Lb	5.945	6.114
L3	Ld	15.190	15.239
I4	Ie	20.487	20.555

has less than about 20 pixels on its boundary.

Next the method is applied to pairs of different season's Landsat data of Hachirogata lake. We choose the spring data is the same as Fig.3 and the summer data is presented in Fig.7. Vegetation area has large seasonal variation. Therefore we use the water bodies as the relatively stable regions for the registration. Owingto the seasonal change of the adjacent regions, the shape of the landmark regions are usually forced to be distorted a bit, however, the water bodies are proved to be useful (Table 4). The pair of complicated shaped regions [1-1'] has about 2.5 times larger MSE_W than the pair [1-a] in Table 1. Actually the shape of the sharp and narrow part is especially different and the boundary length of the [1'] is about 13% shorter than [1]. In spite of the difference, the MSE_W is yet small enough to identify the regions to be matched each other between two images (Table 3).

In urban area, the artificial constructions: buildings, roads, bridges, etc. are useful as the landmark regions. Their shapes are quite stable under the change of seasons. We should mainly pay attention to the permanent change under the passage of time.

We can not compare directly the result of the wavelet and the Fourier descriptor, because the definitions of MSE_W and MSE_F are completely different. However we can still examine their applicability and reliability (Table 5).

The MSE of the Fourier transform MSE_F is not stable for the complicated shaped regions as the MSE of the wavelet transforms MSE_W. Especially it is manifest for the very thin shaped pair [3-c]. The MSE_F is apparently too large. Thus it is not proper for the matching algorithm. The reliability of the MSE_F is higher for round shaped regions and tend to be useless for the region with complicated or "far from round" shape. For the Fourier series the round shape dominates the lower order terms of the Fourier descriptor. A circle means the lowest order term is exact. As in the section 2 we use the lower order
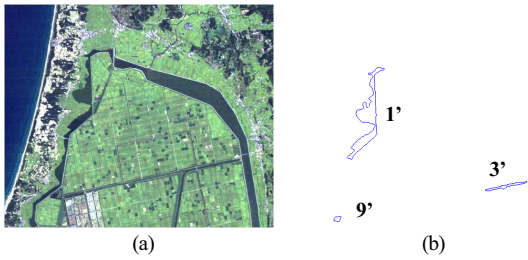
(a)   (b)

Fig.7   Landsat true-color image of Hachirogata lake at 14 Sept. 1992: Summer data (a) and its feature regions (b).

Table.4 MSE_W of the pairs of matched regions between spring and summer Landsat data in Hachirogata lake.

Spring	Summer	MSE_W(Haar)	MSE_W(Daubechies2)
1	1'	3.153	3.161
3	3'	0.866	0.872
9	9'	0.337	0.347

terms $k \leq 2$. It is sufficient for round region, however, very complicated shaped region is theoretically out of range.   Even, including higher order coefficients (k<5), the result does not improve very much.   It is necessary to calculate much higher order terms to have the high reliability as the wavelet transform. It also costs much more computation time. On the other hand, the MSE of the Haar wavelet transform is very stable for various shaped regions, and always less than 4.

5. Conclusion

The registration of remote sensing data which is base on the wavelet transform is found to be stable.   The mean square error by the wavelet is also robust enough to make the clear difference between the matching case and the non-matching case. Therefore, setting the threshold value it can be applied as the automated matching algorithm. The wavelet method is more stable than the Fourier transform method, irrespective of various shapes in remote sensing data.   Thus, the wavelet method is superior to the Fourier method.

We have not found any particular different effect between Landsat and Ikonos yet.   It would be due to the fact that we only use the data after the edge extraction.   We also adopt the segmentation and it gets rid of the high spectral resolution of Ikonos.   The shapes of the extracted objects have no characteristic differences which depend on the spatial resolutions. If we utilize not only the high spatial resolution but also the high spectral resolution, the situation would be more interesting.

Table.5   Comparison between the MSE_W and MSE_F

Original	Test	MSE_W(Haar)	MSE_F(Fourier)
1	a	1.268	4.335
2	b	0.462	0.314
3	c	0.480	188.424
4	d	0.799	3.842
5	e	1.558	1.739
6	f	0.571	0.221
7	g	1.715	0.416
8	h	0.840	0.642
9	i	0.578	2.599

<Reference>

R. Anzai and M. Tomiya, "Registering a Pair of Remote Sensing Image Data using Fourier Descriptor", Journal of Remote Sensing Society of Japan, Vol.21, 2001, 232-239 (in Japanese).

I. Daubechies, "Orthonormal bases of compactly supported wavelets", Communication of Pure and Applied Mathematics, vol. XLIV, 1988, 909-996.

I. Daubechies, "Ten Lectures on Wavelets", SIAM, Philadelphia, 1992.

G. H. Granlund, "Fourier preprocessing for hand print character recognition", IEEE Transaction on Computer, Vol.C-21, 1972, 195-201.

K. K. Simhadri. S.S. Iyengar, R. J. Holyer, M. Lybanon, and J. M. Aachary, Jr., "Wavelet-Based Feature Extraction from Oceanographic Images", IEEE Transanctions on Geoscience and Remote Sebsing, Vol.36, 1998, 767-778.

E. J. Stollnitz, T. D. deRose, D. H. Saleson, "Wavelets for computer graphics – Theory and Applications", Morgan Kaufman, San Francisco, 1996.

Y. –H. Tseng, J.-J. Tzen, K.-P. Tang and S.-H. Lin, "Image-to-Image Registration By Matching Area Feature Using Fourier Descriptors And Neural Networks", Photogrammetric Engineering and Remote Sensing, Vol.63, 1997, 975-983.

C. T. Zahn and P. Z. Roskies, "Fourier descriptors for plane closed curves", IEEE Transaction on Computer, Vol.C-21, 1972, 269-281.